



Cobalt-based nanoparticles strongly diminish CalceinAM fluorescence independently of their cytotoxic potential in human lung cell line

Mohd Javed Akhtar^{a,*}, Maqusood Ahamed^a, Hisham Alhadlaq^b

^a King Abdullah Institute for Nanotechnology, King Saud University, Riyadh 11451, Saudi Arabia

^b Department of Physics and Astronomy, College of Science, King Saud University, Riyadh 11451, Saudi Arabia

ARTICLE INFO

Keywords:

CalceinAM fluorescence quenching
Reactive oxygen species
 O_2^- induction
 Co^{2+} dissolution
Apoptosis
NAC
Oxidative stress

ABSTRACT

Objective: Cobalt nanoparticles (NPs) when released into the air during industrial processes, can enter the lungs through inhalation, leading to potential toxicity and respiratory issues. The mechanism of cobalt toxicity is not well understood and needs further investigation.

Methods: We, therefore, studied the effects of two kinds of cobalt-based nanoparticles (NPs) on lung cells. These NPs were Co NPs (i.e. Cobalt NPs) and Co-Fe NPs (i.e. $CoFe_2O_4$ NPs) that were similar in size and shape but slightly differed for the surface iron composition. The average size of Co NPs was 28 ± 18 nm, and that of Co-Fe was 26 ± 13 nm. We exposed the cells to the NPs for 24 h and measured their viability by MTT assay and CalceinAM fluorescence imaging. Potential induction of reactive oxygen species (ROS) was detected by probes DHE specific for superoxide (O_2^-) and DCFH-DA for hydrogen peroxide (H_2O_2). Antioxidant glutathione (GSH) quantification was followed by measuring apoptotic/necrotic potential.

Results: Using Co NPs and Co-Fe NPs, we measured the IC50 for cell growth in A549 cells after 24 h of exposure. The values were 79 $\mu g/mL$ and 163 $\mu g/mL$, respectively. We also observed that both NPs induced ROS and reduced the fluorescence of CalceinAM in the cells, but Co NPs had a stronger effect than Co-Fe NPs. This was correlated with the production of O_2^- by the NPs, which was higher for Co NPs than for Co-Fe NPs. On the other hand, H_2O_2 production was higher for Co-Fe NPs than for Co NPs. Our study suggests that the main cause of differential O_2^- production is the differential release Co^{2+} ion due to surface modification resulting in differential quenching of green (CalceinAM) fluorescence by both NPs. Both NPs induced apoptosis mode of cell death.

Conclusion: Our data from the use of naïve and surface-modified cobalt-based NPs, suggest that NAC can protect cells from cobalt-based NP toxicity by not only restoring cellular GSH levels but also by chelating released Co^{2+} ions from the NPs surfaces. Additionally, this study for the first time to our knowledge indicates that CalceinAM alone is not sufficient to assess the toxicity of cobalt-based NPs. Other methods should be used to confirm the cytotoxicity data of cobalt-based NPs.

1. Introduction

Nanotechnology is the material science of precise manipulation of matter at the size of molecules or macromolecules, say sizes that are below 100 nm (Yang et al., 2019). Materials at the nanoscale (average size of 1–100 nm) have provided numerous opportunities in the fields of catalysis and medicine (Yang et al., 2019). Cobalt-based nanoparticles (NPs) are receiving significant attention due to their exploitable properties in catalytic and biomedical applications (Ahamed et al., 2016). Cobalt NPs are entering many industrial applications due to their intrinsic properties. Cobalt-based NPs can be used for catalysis,

pigments, sensors, magnets, electrochemical devices, and energy storage systems (Kong et al., 2020). Their widespread use increases the chances of exposure making cobalt-based particles and NPs risky to living beings and their ecosystem. Co (atomic number 27) can exist in numerous oxidation states, including +2, +3, -1, and +6 (Kobayashi and Shimizu, 1999). Like other trace metals, Co is part of many enzyme systems which are essential for the normal functioning of living organisms (Kobayashi and Shimizu, 1999). Cobalt is, therefore, an important redox reactive metal that can take part in redox reactions either by accepting or donating electrons to other molecules present either in a chemical system or biological system (Kobayashi and Shimizu, 1999). In addition,

* Corresponding author at: King Abdullah Institute for Nanotechnology (KAIN), King Saud University, P.O. Box 2454, Riyadh 11451, Saudi Arabia.

E-mail address: mjakhtar@ksu.edu.sa (M.J. Akhtar).

<https://doi.org/10.1016/j.jksus.2023.102987>

Received 28 August 2023; Received in revised form 20 September 2023; Accepted 31 October 2023

Available online 1 November 2023

1018-3647/© 2023 The Author(s). Published by Elsevier B.V. on behalf of King Saud University. This is an open access article under the CC BY-NC-ND license (<http://creativecommons.org/licenses/by-nc-nd/4.0/>).

cobalt oxide particles are generated as a result of combustion, and these particles get airborne (Sabbioni et al., 2014). Once airborne, these particles can enter the lungs of humans and other terrestrial animals (Sabbioni et al., 2014). Cobalt particles in their nano-scale form can potentially cause damaging effects on human health. The solubility of cobalt varies greatly in aqueous media, ranging from the high solubility of metallic cobalt to almost no solubility of oxide forms.

Co NPs have been reported to cause DNA damage and oxidative stress in several reports (Akhtar et al., 2017; Wan et al., 2012). However, the precise mechanism of inducing toxicity by Co-based NPs is still unclear. Inducing toxicity involves the internalization of NPs into tissues and the dissolution of Co NPs into Co^{2+} in media (Chattopadhyay et al., 2015; Kong et al., 2020). Cobalt NPs induce inflammation in mice by upregulating Tau protein phosphorylation (Li et al., 2021). The cobalt NPs also generated ROS in BV2 microglial cells by activating the enzyme NADPH oxidase 2 (Li et al., 2021). Humans occupationally exposed to cobalt NPs have been found to have significant impairments in cognitive function and memory loss (Gieré, 2016). In addition, Co NPs exposure resulted in significant damage to the cell membrane and mitochondria of HHSY5Y neurons, followed by an increase in ROS levels, as well as oxidative stress and hypoxia-induced factor-1 (Zheng et al., 2021). Several human diseases, such as pulmonary fibrosis, interstitial pneumonitis, and asthma, have been linked to cobalt particle exposure (Kong et al., 2020). Cobalt-based NPs have been studied in a wide variety of organisms and are considered probable carcinogens in humans (Sabbioni et al., 2014). As Co oxides are extremely insoluble and Co ions are highly dissolvable (Sabbioni et al., 2014), we believe that dissolution may be a potential mechanism for the toxicity caused by Co-based NPs.

Leached out Co^{2+} from cobalt-based NPs can accumulate inside cells causing unwanted interactions with cell components, often disrupting cellular redox balance as a result. To determine the effect of varying dissolution on cellular activity, we chose two types of cobalt-based NPs with similar sizes and shapes except for some differences in chemical composition that could lead to differential leaching of Co^{2+} ions. We selected cobalt NPs (Co NPs) and cobalt ferrite (CoFe_2O_4 NPs or simply Co-Fe NPs for) and proceeded by evaluating cell viability due to the exposure of Co NPs and Co-Fe NPs for 24 h in human lung epithelial (A549) cells utilizing methods like MTT, NRU, CalceinAM fluorescence and phase-contrast microscopy. ROS inducing potential of the two NPs was determined by two probes; DHE which specifically detects O_2^- and DCFH₂DA which largely determines H_2O_2 . The use of these probes can provide more insight into how they alter cellular oxidative stress levels. Other oxidative parameters included in this study were the determination of intracellular ubiquitous antioxidant glutathione (GSH), lipid peroxidation (LPO), and lactate dehydrogenase (LDH) release in surrounding culture media. Mode of cell death mediated by Cobalt-based NPs has been reported to vary with types of cells, therefore, we also included measurements to determine the mode of cell death such as triple staining by annexin-V FITC/PI/Hoechst and activity of caspase 9 and caspase 3 enzymes. A549 cells are a type of human lung cancer cell line that has been used in various studies related to lung cancer research (Ahamed et al., 2017; Fahmy et al., 2020). Many low molecular weight antioxidants such as GSH, N-acetyl cysteine (NAC), flavonoids, and vitamin E are strong chelators of metal ions and, therefore, can protect cells against damage caused by metal-induced oxidative stress (Jomova and Valko, 2011). In this study, therefore, we investigated the potential role of NAC in protecting cells from the harmful effects of metal ions released by NPs exposure either by chelation and/or restoring thiol content (like GSH) of cells.

2. Materials and methods

2.1. Chemicals and reagents

Fetal bovine serum, CalceinAM, and penicillin–streptomycin were purchased from Invitrogen Co. (Carlsbad, CA, USA). DMEM F-12, MTT

[3-(4,5-dimethyl thiazol-2-yl)-2,5-diphenyl tetrazolium bromide], NADH, pyruvic acid, perchloric acid, hydroethidine (DHE), DCFH-DA, GSH, o-phthalaldehyde (OPT), hank's balanced salt solution (HBSS), caspase substrates, and Bradford reagent were obtained from a commercial source (Sigma–Aldrich, MO, USA). An apoptosis/necrosis triple staining kit was obtained from BD Biosciences (USA). Ultrapure water was taken from a Milli-Q system (Millipore, Bedford, MA, USA). All other chemicals used were of reagent grade.

2.2. NPs of cobalt and cobalt ferrite

NPs of Cobalt (Co), and Cobalt Ferrite (CoFe_2O_4 or simply as Co-Fe) were purchased from Sigma-Aldrich (MO, USA). All NPs were obtained and stored in powder form for later use. As per the information provided by the supplier, the average sizes of Co NPs were 28 ± 18 nm whereas that of Co-Fe was 26 ± 13 nm. Before biochemical studies of these NPs, we have characterized these NPs by conducting various characterizing techniques as described in previous publications (Ahamed et al., 2016; Akhtar et al., 2017).

2.3. NPs dissolution

NPs dissolution was determined as outlined elsewhere (Sabbioni et al., 2014). Briefly, NPs of Co and Co-Fe each at the concentration of 1 mg/mL were suspended in the aqueous media of interest and left for the incubation of 1 week with gentle shaking for 1 h/day on a shaker. After 1 week of incubation, each suspension of each NP was centrifuged at $10000 \times g$ for 10 min. Now free Co^{2+} was measured in the supernatant collected after centrifugation in the atomic absorption spectroscopy (AAS). $\text{CoCl}_2 \cdot 6\text{H}_2\text{O}$ was used in preparing standards of Co^{2+} (Akhtar et al., 2010).

2.4. MTT and CalceinAM assays

A549 cells (ATCC, US) were cultured in DMEM media and added with 10 % fetal bovine serum (FBS) and antibiotic/antimycotic solution. Cells were passaged according to standard procedure. Cells were exposed to NPs for a 24 h exposure. After the exposure period was over, the media aspirated off and a 100 μL MTT solution prepared in HBSS was added and incubated for 2 h. The degree of MTT conversion to blue formazan was calculated in % of cell viability where 100 % cell viability was considered for control cells. Similarly, control and treated cells were labeled with CalceinAM for 1 h after exposure periods were completed. The final concentration of Calcein-AM was 5 μM in a 96-well plate. Cells labeled with CalceinAM were counterstained with a Hoechst probe for the purpose of control fluorescence as explained in the results.

2.5. Determination of lipid peroxidation and membrane integrity

Lipid peroxidation was detected by the method of Ohkawa et al that uses thiobarbituric acid as a probe for malondialdehyde (MDA) (Ohkawa et al., 1979). MDA is one of the several end products that arise as a result of LPO in polyunsaturated fatty acids constituting cell membranes. It is quantified as thiobarbituric acid reactive substances (TBARS) at 532 nm of absorbance. LPO results in damage to membranes that make cell membranes leaky for intracellular contents. One of the easily quantifiable substances is the enzyme lactate dehydrogenase which catalyzes the conversion of pyruvate to lactate in the metabolism. LDH is easily detected by a decrease in the absorbance of NADH at 340 nm as described (Welder, 1992).

2.6. Determination of O_2^- and H_2O_2 as the primary member of ROS

ROS has a key role in cell signaling at low concentrations but can result in oxidative stress at high concentrations enough for the nullifying capacity of the cell. Moreover, cell signaling and oxidative stress are

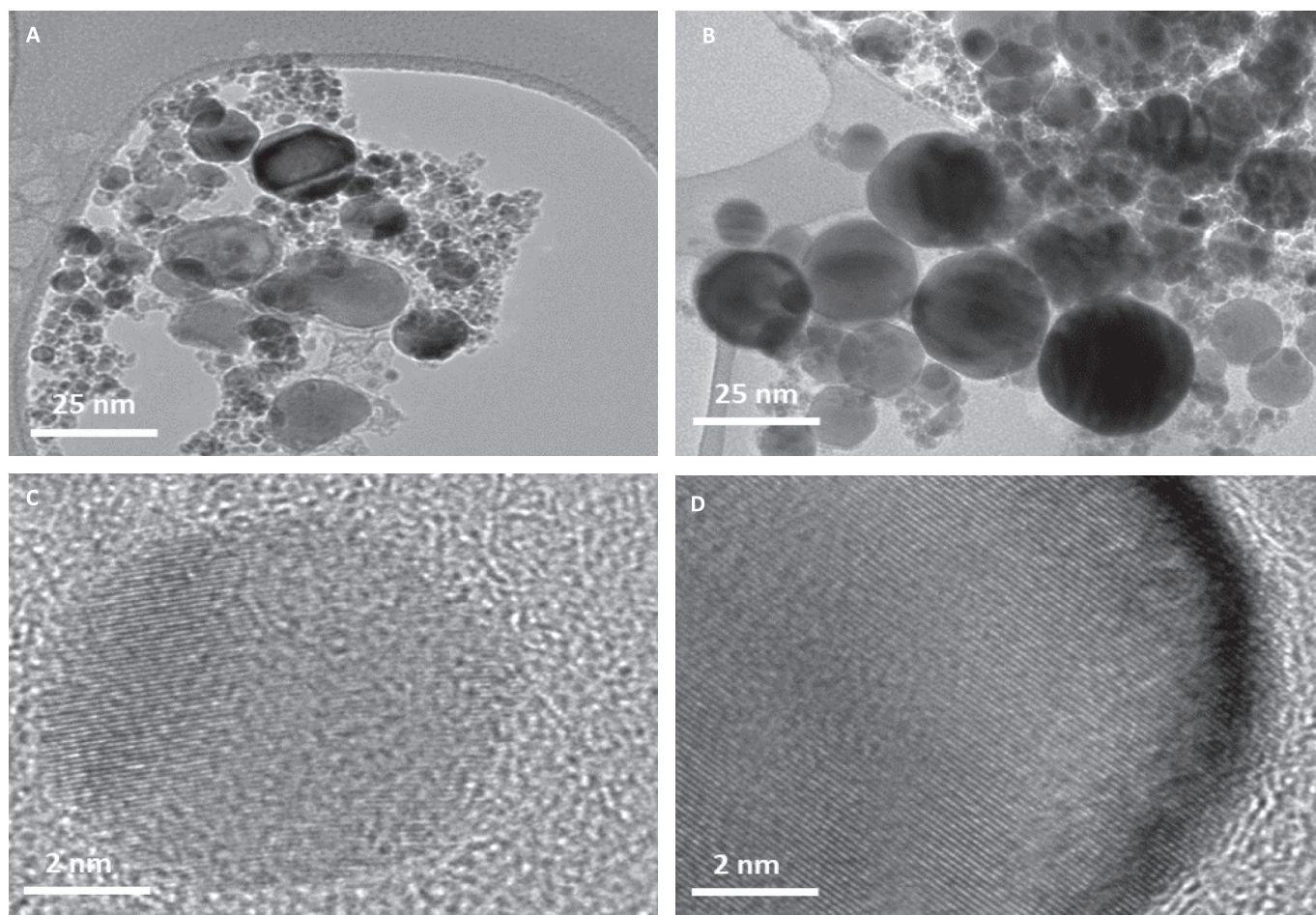


Fig. 1. NPs of cobalt (Co NPs) and cobalt ferrite (Co-Fe NPs) were captured by transmission electron microscope (TEM). TEM images are provided in (A) and (B) respectively. HR-TEM images captured at 2 nm resolution are shown in (C) and (D) depicting a lattice pattern typical of crystal structure.

dependent on the specific ROS, their primary site of production, and the types of cells. O_2^- which is mostly produced by mitochondria and the precursor of H_2O_2 was detected by DHE probe at $5 \mu M$ of final concentration incubated for 30 min after completion of exposures. The same cells were also co-labeled with DCFH-DA at the final concentration of $10 \mu M$ for 30 min. Cells were imaged under a fluorescence microscope using appropriate filters as described previously (Akhtar et al., 2022).

2.7. Determination of intracellular GSH content

Control and treated cells were lysed in distilled water by three cycles of freeze–thaw. Cell lysate, thus, obtained was centrifuged at $10,000 \times g$ at $4^\circ C$. Supernatant was analyzed for total GSH level by a fluorescent thiol-reacting probe *ortho*-phthalaldehyde (OPT) as described previously (Akhtar et al., 2015). The cell lysate was also used to determine protein concentration and GSH content was presented as GSH/mg protein.

2.8. Analysis of cell death pathways

A triple staining approach was taken to assess the health status of cells as described in several publications (Akhtar et al., 2023; Atale et al., 2014). This approach involved using a universal cell-permeable dye, Hoechst 33342, to label healthy cells with blue fluorescence. Apoptotic or necrotic cells were identified by a combination of green annexin-V staining and red PI staining (Crowley et al., 2016; Sawai and Domae, 2011). In addition to direct analysis of cell health, we also indirectly estimated the activity of caspases 3 and 9 in the cells. Cells (5×10^4)

were grown for 24 h and got exposed to the IC₅₀ of NPs for another 24 h. Cells were then collected, washed, and lysed to measure enzyme activities. Caspase 3 and 9 activities were measured using substrates Ac-DEVD-AFC and Ac-LEHD-AFC, respectively. Enzymatic reactions were conducted by combining $20 \mu L$ of the enzyme-specific substrate, $30 \mu L$ of cell lysate from each cell, and $150 \mu L$ of enzyme buffer (50 mM Hepes, 1 mM EDTA, and 1 mM DTT, pH 7.2) for 20 min. Readings were taken at 5-minute intervals using a plate reader (Synergy HT, Bio-Tek, Winooski, Vermont, USA). The activities of caspases were expressed as a percentage of the control.

2.9. Protein estimation

The total protein content was measured by a convenient BCA Protein Assay Kit from Sigma-Aldrich as per instructions.

2.10. Statistics

ANOVA (one-way analysis of variance) followed by Dunnett's multiple comparison tests were employed for statistical analysis of results. For a particular set of experiments, a burst of images was captured at the constant exposure of time, gain, saturation, and gamma. For the calculation of corrected total cellular fluorescence (CTCF), a reasonably constant area was selected and restored in all images once opened during analysis via the 'restore selection' command present in ImageJ software (NIH, Bethesda, MD, USA).

Table 1
Summary of the physico-chemical properties of NPs of Co and Co-Fe.

Parameter	Co NPs	Co-Fe NPs
TEM	28 ± 18 nm	26 ± 13 nm
SEM	Spherical	Spherical
Crystallinity	Crystal	Crystal
NPs dissolution in culture media	24.7 ± 5.3 %	15.3 ± 4.5 %
NPs dissolution in PBS	9.3 ± 4.1 %	4.8 ± 2.6 %

3. Results

3.1. The dissolution of Co^{2+} was higher in the suspension of Co NPs as compared to that in the suspension of Co-Fe NPs

TEM was employed to determine the morphology and size distribution of NPs (Fig. 1). The images obtained showed that both Co and Co-Fe NPs had a spherical shape with a well-defined size (Fig. 1A and 1B). The average size of Co NPs was found to be 28 ± 18 nm and the size of Co-Fe was found to be 26 ± 13 nm, which matched with the information provided by the supplier. Table 1 summarizes NPs sizes and degree of dissolutions carried out in culture media and phosphate buffer saline (PBS). This observation could be attributed to several factors

like NPs composition, the presence of organic molecules in suspending media for the NPs may be counted as prominent ones. The presence of Fe in the Co-Fe NPs may have hindered the dissolution of Co^{2+} .

3.2. Co NPs were more toxic than the Co-Fe NPs

The toxicity of Co NPs is significant, with effects starting at 25 $\mu\text{g}/\text{mL}$ (as shown in Fig. 2A). Both types of NPs were found to have a concentration-dependent effect on A549 cells. However, the cytotoxicity data clearly indicates that Co NPs are more toxic than Co-Fe NPs. The IC50 for Co NPs was calculated to be 79 $\mu\text{g}/\text{mL}$ after 24 h of exposure, while for Co-Fe NPs it was 163 $\mu\text{g}/\text{mL}$. Fig. 2B shows phase-contrast images of cells treated with IC50s of the two NPs, which exhibit significant deviation in cell morphology from the control cells. The treated cells appear to have similar changes in cell size and shape, with a tendency to adhere strongly to the culture vessel surface.

3.3. CalceinAM fluorescence suppression was proportional to Co^{2+} leaching

The fluorescence of CalceinAM was found to be significantly different for the two types of NPs (NPs). This study is the first to explore

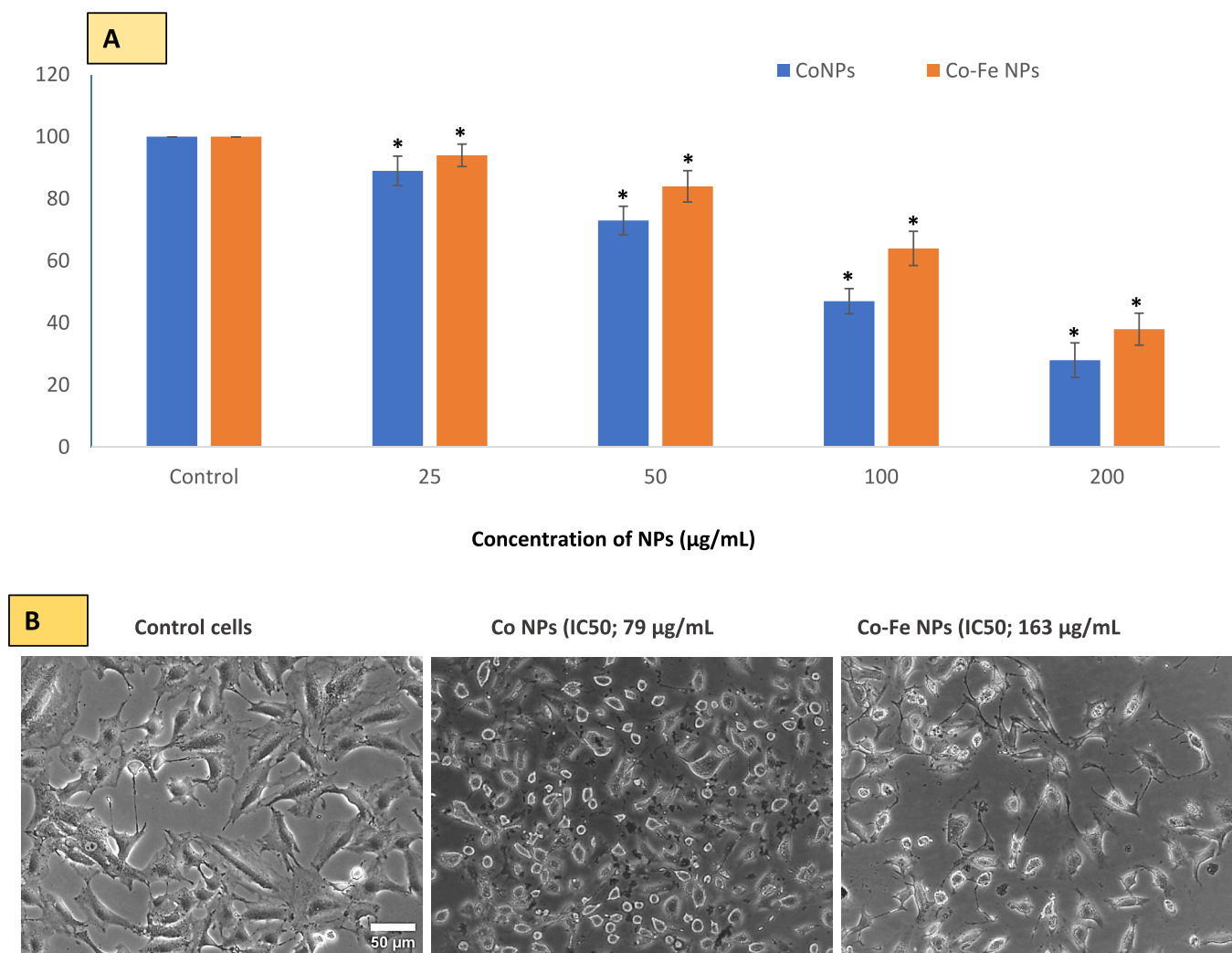


Fig. 2. In A549 cells, MTT bioassay was used to evaluate cell viability due to Co NPs and Co-Fe NPs exposure. The two NPs reduced cell viability in A549 cells in a concentration-dependent manner at the concentration ranges provided in Figure (A). The online calculator (<https://www.aatbio.com/tools/ic50-calculator>) (accessed on 5 April 2023) was used to calculate the concentration of NPs that inhibit/reduce cell growth by 50 (i.e. IC50). Fig B is a phase contrast image of control and IC-50 treated cells. The data represent three identical experiments (n = 3) conducted in triplicate. *Statistically significant difference ($p < 0.05$) from control.

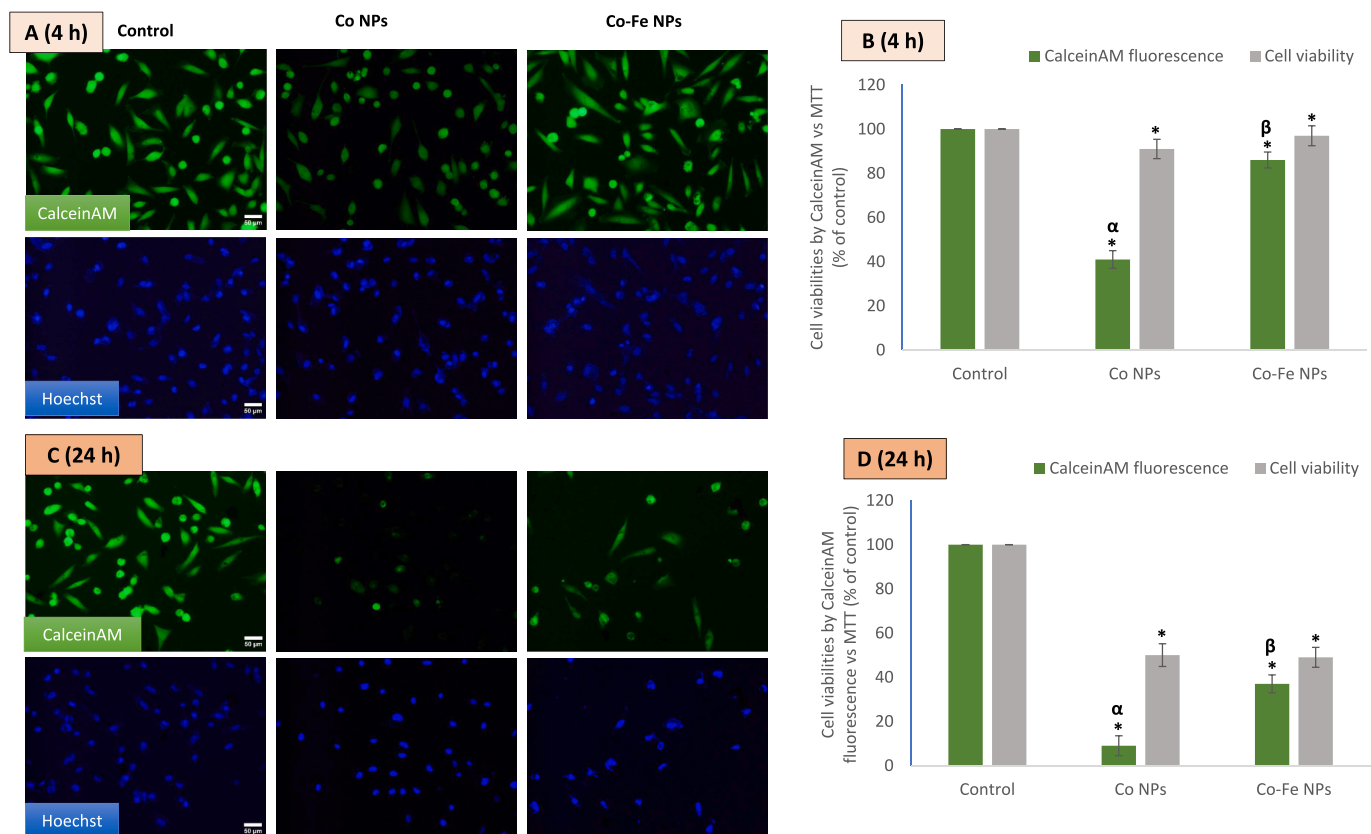


Fig. 3. Shows the results of an experiment where A549 cells were treated with IC50 concentrations of the two variants of cobalt-based NPs. The cells were then imaged using Calcein-AM and Hoechst co-labeling for 4 h (A and B) and 24 h (C and D). The data represent three identical experiments (n = 3) conducted in triplicate. *Statistically significant difference (p < 0.05) from control. The α and β symbols represent a significant decline in CalceinAM fluorescence as compared to the cytotoxicity value obtained by MTT at IC50 concentrations of NPs of Co and Co-Fe respectively.

the effect of cobalt NPs on the quenching of CalceinAM fluorescence, as well as the comparative mechanism of toxicity of Co NPs in bare form and Co NPs in coated form with Fe element. A time-dependent quenching potential of the two NPs was determined, and it was found that while Co NPs started quenching even at 2 h of exposure, Co-Fe did not quench CalceinAM fluorescence before 4 h of exposure. Therefore, an additional short 4-hour exposure was included for CalceinAM fluorescence measurement (Fig. 4A) in addition to 24 h of exposure (3B) carried out in each experiment.

Cell viability was measured by CalceinAM fluorescence and compared to the MTT bioassay method. Hoechst staining was used as a control of fluorescence (Fig. 3A and B), and its fluorescence (blue-colored images) was relatively uniform in each group compared to fluctuating CalceinAM fluorescence. The results showed that the CalceinAM fluorescence remaining after quenching was 41 % and 9 % after 4 h (Fig. 3C) and 24 h (Fig. 3D) of exposure to bare Co NPs, respectively. However, the same values were 86 % and 37 % in the case of Fe-containing Co (Co-Fe) NPs treatment, indicating a significant reduction in Co²⁺ leaching from Fe-containing Co-Fe NPs compared to Co NPs. In other words, the reductions in cell viability due to exposure to the two cobalt-based NPs were not as severe as the reduction in CalceinAM fluorescence.

3.4. Cobalt-based NPs induce high concentrations of O₂⁻ and H₂O₂ within cells

The production of reactive oxygen species (ROS) is considered the primary mechanism of nanoparticle toxicity, and this can occur as early as 1–4 h into the incubation period. The degree of ROS induction and the cell type can affect the length of time it takes for ROS production to

occur. To accurately measure ROS, a short 4-hour exposure was included in addition to the final 24-hour exposure time. Dyes specific to O₂⁻ and H₂O₂ were co-labeled and imaging was conducted (Fig. 4A and B). The fluorescent data extracted from images (Fig. 4C and D) suggest that Co NPs have the potential to induce O₂⁻ at 4 h of exposure but not H₂O₂. However, at 24 h of exposure, Co NPs caused the induction of both O₂⁻ and H₂O₂. In the case of iron-containing Co-Fe NPs, H₂O₂ was significantly higher than the control at both 4- and 24-hour exposures. Co-Fe NPs also generated O₂⁻ at both exposure periods, but with lower intensity than Co NPs. The iron in Co-Fe may play a catalyzing role (like the Fenton reaction) in the higher generation of H₂O₂ compared to only Co NPs.

3.5. NPs induce apoptosis mode of cell death

The A549 cells that were treated underwent extensive staining with PI and annexin V as evidenced in live-cell images provided in (Fig. 5). It is important to note that cells undergoing apoptosis display intact cell membranes with blebs, as well as a reduction in volume and tightly packed chromatin that emits bright and clumped fluorescence which is present in images of cells treated with both types of NPs. In contrast, cells undergoing necrosis exhibit early cell membrane damage, an increase in cell volume, and the dilated nuclear periphery with circumscribed chromatin that gives off diffused fluorescence and a preferential uptake of PI over annexinV-FITC (Fig. 5A). In live cell images of triple staining, it is hard to observe the aforementioned evidence of necrosis. Additionally, activated levels of caspases 9 (5B) and 3 (5C) serve as further evidence of apoptosis in A549 cells. Overall, data suggest cobalt-based-NPs be apoptotic in A549 cells.

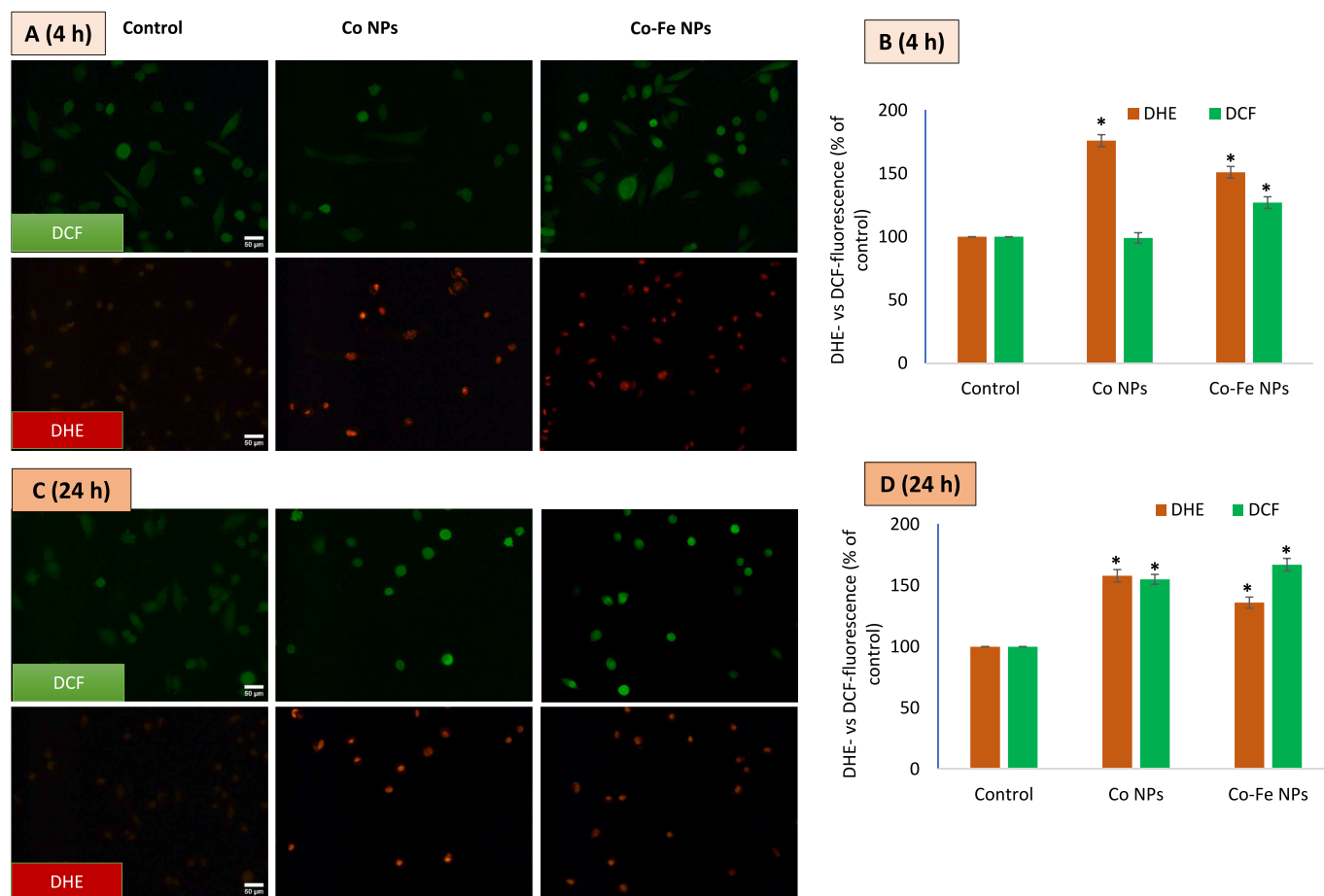


Fig. 4. Presents the results of an experiment where A549 cells were treated with IC50 concentrations of different variants of cobalt-based NPs. The cells were then imaged using DCFH-DA and DHE co-labeling for 4 h (A) and fluorescence intensity quantified (B). C and D refer the same for a and 24 h exposure. The data represent three identical experiments (n = 3) conducted in triplicate. *Statistically significant difference (p < 0.05) from control.

3.6. Co NPs induced oxidative stress, and exogenous NAC prevented GSH exhaustion and inhibited quenching of CalceinAM fluorescence

In addition to inducing ROS, NPs (NPs) also cause lipid peroxidation (as shown in Fig. 6A) and degradation of membrane integrity (as shown in Fig. 6B). However, the addition of N-acetylcysteine (NAC) significantly prevented the depletion of the intracellular antioxidant glutathione (GSH) caused by NPs exposure (as shown in Fig. 6C). It is worth noting that NAC has been reported to chelate metal ions, which could explain the significant restoration of CalceinAM fluorescence (as shown in Fig. 6D and E) that was previously quenched by Co^{2+} . This finding suggests that NAC can protect cells by reducing oxidative stress, restoring GSH levels, and chelating metal ions such as Co^{2+} . Therefore, the application of NAC is crucial for managing and designing experiments involving metal ions like Co^{2+} .

4. Discussion

The two cobalt based NPs used in this study were largely similar except for the iron surface coating on one NPs. This iron coating resulted in significant reduction of Co^{2+} leaching but increased the iron content in modified NP. As would be expected, the iron component in Co-Fe NP could have resulted in less dissolution of Co^{2+} in comparison to pure Co NPs. Surface tuning of NPs involves various strategies such as coating, functionalization, doping, or alloying that can modify the physico-chemical and biophysical characteristics of NPs (Akhtar et al., 2022; Lateef et al., 2023). These modifications can influence the interactions of NPs with biological systems, such as cells, tissues, organs, or organisms,

and affect their biodistribution, biocompatibility, bioactivity, and biodegradability (Freese et al., 2012; Rivet et al., 2012; Sukhanova et al., 2018). Cytotoxicity data obtained in this study by MTT assay clearly indicates that Co NPs are more toxic than Co-Fe NPs. This data, however, is not correlated with the toxicity data obtained by live-cell imaging via CalceinAM. Though Co^{2+} ions have been reported to diminish CalceinAM fluorescence (Petronilli et al., 1998) but this is the first study that found a similar finding for cobalt-based NPs as well. Quenching of live-cell dye CalceinAM by Co NP exposure was steeper than it would be suggested by cytotoxicity data acquired by alternative methods like MTT assay.

NPs can trigger cytotoxicity in cells by producing reactive oxygen species (ROS). Cobalt can generate ROS by reducing O_2 directly on its particle surface whereas Co^{2+} (or any transition metal ion) can produce powerful oxidant hydroxyl radical ($\cdot\text{OH}$) in the presence of mild oxidant H_2O_2 (Turrens, 2003). $\text{O}_2^{\cdot-}$ and H_2O_2 are relatively stable ROS and have mild reactivity suited for engaging in signaling functions in comparison to $\cdot\text{OH}$ which is one of the most powerful oxidants in nature (Turrens, 2003). Hydroethidine (DHE) was utilized to detect $\text{O}_2^{\cdot-}$ which is a parental molecule for the formation of other ROS such as H_2O_2 and $\cdot\text{OH}$ radical. Moreover, transition metal-induced generation of $\cdot\text{OH}$ in close association with DNA has been proposed as the central mechanism of damaging DNA as positively charged Co^{2+} are attracted toward negatively charged DNA molecules (Turrens, 2003; Yamada, 2013). Therefore, $\cdot\text{OH}$ generated in the vicinity of DNA can attack bases leading to the reported carcinogenicity of Co^{2+} (Turrens, 2003; Yamada, 2013). Overall, data on DHE and DCF fluorescence suggest that Co NPs primarily induce $\text{O}_2^{\cdot-}$ which could have been dismutated to H_2O_2 in the

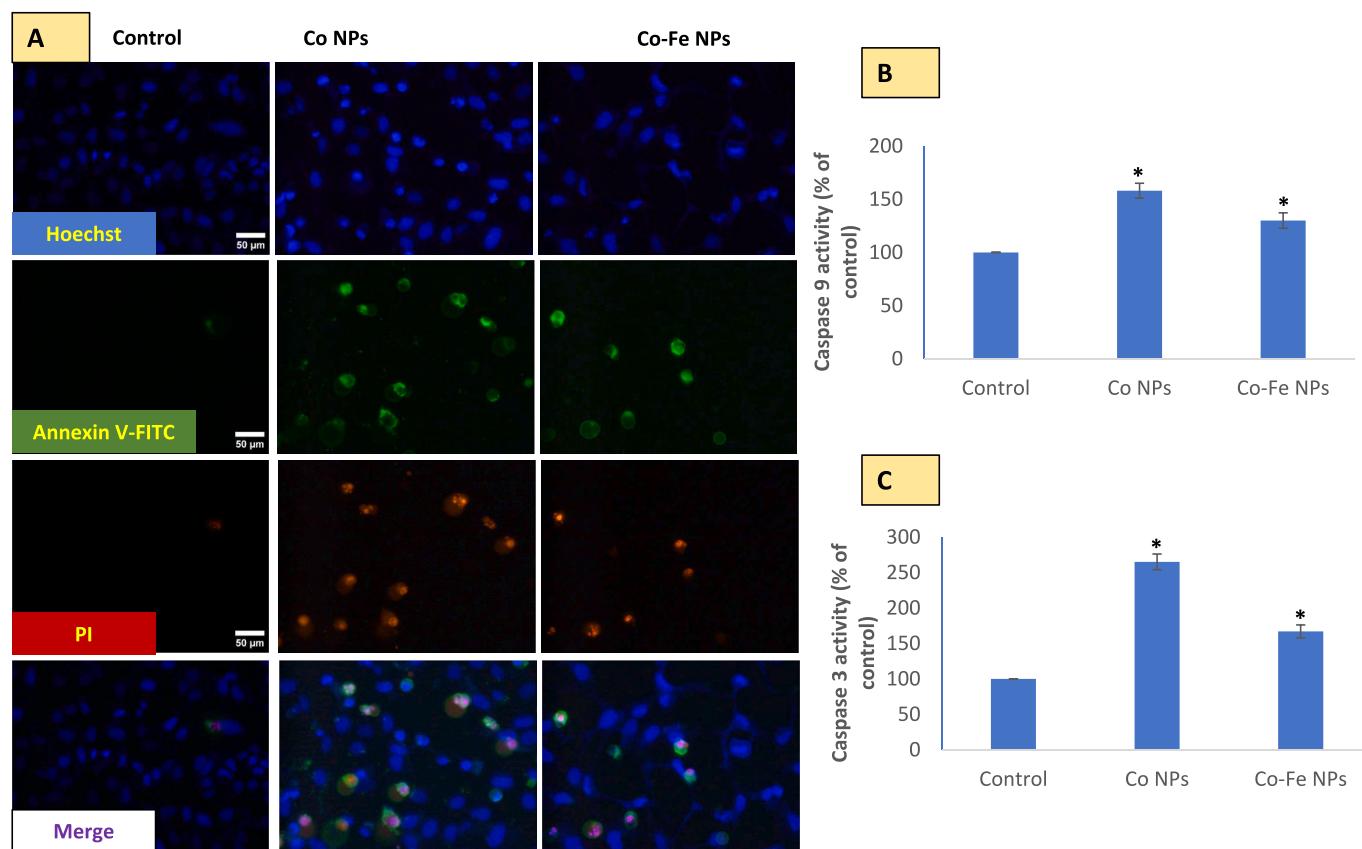


Fig. 5. Shows a potential disbalance between oxidants generation and antioxidant depletion due to exposure to cobalt-based nps. this canlead to lipid peroxidation (LPO) and lactate dehydrogenase (LDH) release, as seen in Fig A and B, respectively. The antioxidant capacity of N-acetylcysteine (NAC) as a precursor of glutathione (GSH) and chelator of oxidant-inducing metal ions is shown in Fig C. Figure D demonstrates the chelation of metal ions by NAC, which prevents quenching of CalceinAM fluorescence by Co^{2+} , as quantified in Figure E. The data represented are mean \pm SD of three identical experiments ($n = 3$) made in triplicates, with * denoting a statistically significant difference from the control ($p < 0.05$). The α and β symbols indicate significant prevention in quenching of CalceinAM fluorescence in the presence of 2 mM exogenously applied NAC along with NPs as compared to that by NPs of Co and Co-Fe alone, respectively.

presence of higher iron of Co-Fe NPs; Co-Fe NPs exhibits a higher potential for H_2O_2 production as indicated by higher DCF fluorescence in comparison of DCF fluorescence due to Co NPs exposure. These results could have important implications in the approaches adapted for NPs modification. Our study on ROS evaluation suggest that the production or suppression of a specific ROS can be achieved by modifying a NP with either a transition metal or a non-transition metal. This can result in significant changes in the NP's properties and interactions with biological systems.

While several studies report apoptotic mode of cell death by cobalt exposure, there are reports on autophagy induction and necrotic mode of cell death as well (Battaglia et al., 2009; Muñoz-Sánchez and Cháñez-Cárdenas, 2019). In this study, the mode of cell death was determined directly by triple staining under the microscopy method as well as the biochemical method as reported (Akhtar et al., 2020, 2023; Atale et al., 2014). Cells undergoing apoptosis exhibit conserved morphological features like shrinkage in cell volume and membrane blebbing. Biochemical staining can further be used to decipher apoptosis from necrosis on grounds of preferential staining of annexinV-FITC that binds with flipped-out phosphatidylserines in the outer cell membrane during apoptosis for recognition and getting cleared by phagocytes (Fadok et al., 2000, 1998). Later on, PI can enter the cells as a result of ongoing disintegration in the nuclear membrane. In necrosis, however, PI preferentially enters cells undergoing necrosis. Staining of annexin V-FITC and PI together is usually indicative of late stages in apoptosis (Sawai and Domae, 2011). Apoptotic cells can further be identified as discrete fluorescence emitted by DNA-binding probes like Hoechst and PI as chromatin material is discretely present in apoptotic cells as a result of

various enzymatic activities activated under apoptosis (Crowley et al., 2016; Sawai and Domae, 2011).

Many low molecular weight antioxidants such as GSH, NAC, flavonoids, and vitamin E are strong chelators of metal ions and, therefore, can protect cells against damage caused by metal-induced oxidative stress (Ahamed et al., 2023; Jomova and Valko, 2011). We found an inhibition by NAC on calceinAM fluorescence suppression. This provides a proof-of-concept that NAC's antioxidation mechanism of replenishing cellular thiols can be complemented by its ability to bind transition metals like Co^{2+} . These findings hold significant implications for the development of therapeutic interventions that can mitigate the harmful effects of metal exposure in cells. Further research is necessary to elucidate the mechanisms underlying NAC's binding properties and its potential applications against toxicity induced by NP exposure in clinical settings.

5. Conclusion

Despite similar in size and shape of cobalt-based NPs studied in this report, data suggests that differences in chemical composition can have a significant impact on the NPs' dissolution and subsequent effects on cells. Although, CalceinAM fluorescence is a reliable and direct way to observe live cells, but our study indicates that CalceinAM alone is not sufficient to assess the toxicity of cobalt-based NPs. Other methods should be used to confirm the cytotoxicity data of cobalt-based NPs. Data in this report also suggest that NAC can have multifaceted nature of antioxidant mechanism when it comes to exposure of NPs that could furnish ions like Co^{2+} . In conclusion, understanding the impact of

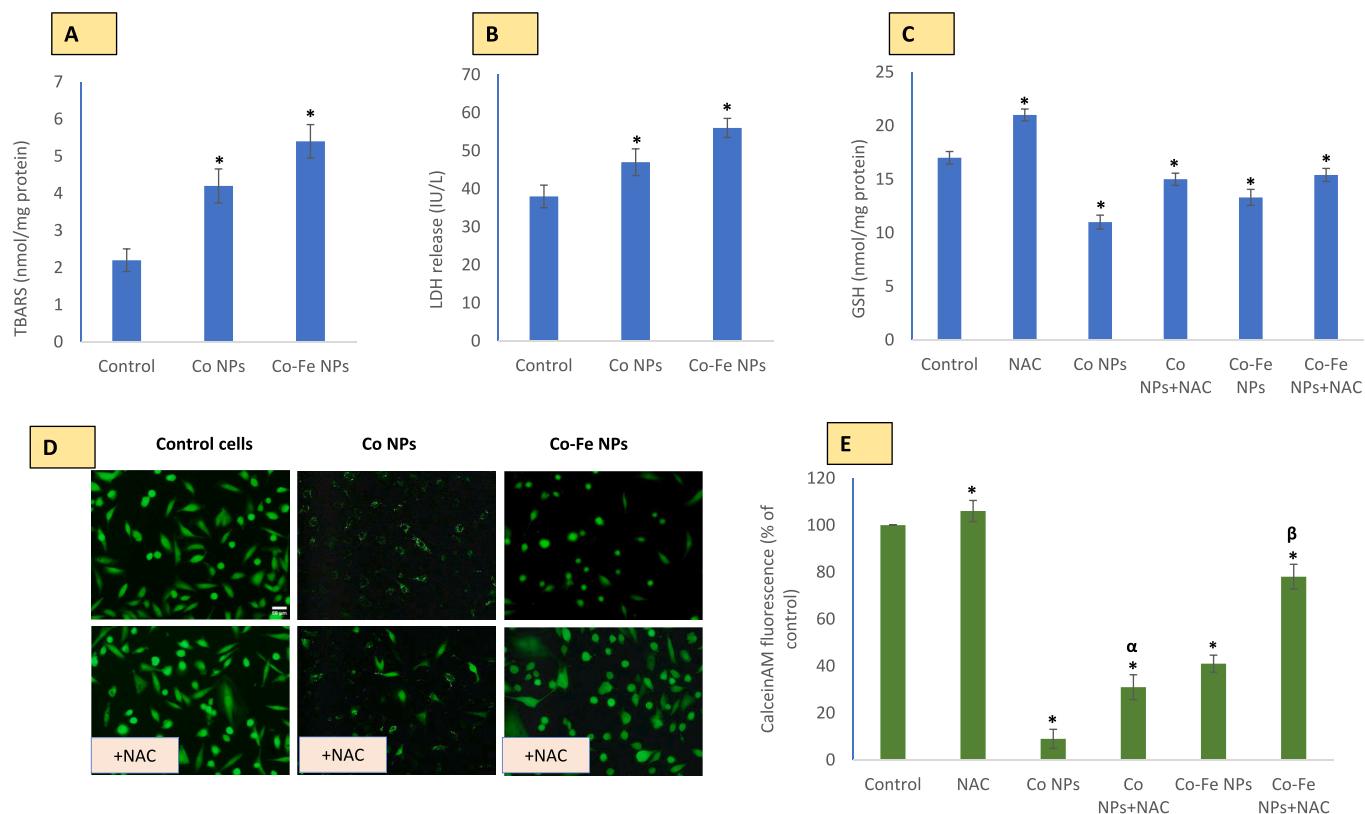


Fig. 6. shows the mode of cell death induced by each variant of cobalt-based NPs in A549 cells. Triple staining (A) and detection of caspase 9 (B) and caspase 3 (C) activities were used to determine cell death. The data represented are mean \pm SD of three identical experiments ($n = 3$) made in triplicates, with * denoting a statistically significant difference from the control ($p < 0.05$ for each).

chemical composition on the behavior and effects of NPs is essential to develop safe and efficient nanomedicines and nanotechnologies.

Declaration of Competing Interest

The authors declare that they have no known competing financial interests or personal relationships that could have appeared to influence the work reported in this paper.

Acknowledgment

The authors extend their appreciation to the Deputyship for Research and Innovation, "Ministry of Education" in Saudi Arabia for funding this research (IFKSUOR3-529-1).

References

- Ahamed, M., Akhtar, M.J., Khan, M.A.M., Alhadlaq, H.A., Alshamsan, A., 2016. Cobalt iron oxide nanoparticles induce cytotoxicity and regulate the apoptotic genes through ROS in human liver cells (HepG2). *Colloids Surf. B Biointerfaces* 148, 665–673. <https://doi.org/10.1016/j.colsurfb.2016.09.047>.
- Ahamed, M., Akhtar, M.J., Khan, M.A.M., Alhadlaq, H.A., Aldalbah, A., 2017. Nanocubes of indium oxide induce cytotoxicity and apoptosis through oxidative stress in human lung epithelial cells. *Colloids Surf. B Biointerfaces* 156, 157–164. <https://doi.org/10.1016/j.colsurfb.2017.05.020>.
- Ahamed, M., Javed Akhtar, M., Majeed Khan, M.A., Alhadlaq, H.A., 2023. Protocatechuic acid mitigates CuO nanoparticles-induced toxicity by strengthening the antioxidant defense system and suppressing apoptosis in liver cells. *J. King Saud Univ. - Sci.* 35 (3), 102585.
- Akhtar, M.J., Ahamed, M., Kumar, S., Siddiqui, H., Patil, G., Ashquin, M., Ahmad, I., 2010. Nanotoxicity of pure silica mediated through oxidant generation rather than glutathione depletion in human lung epithelial cells. *Toxicology* 276, 95–102. <https://doi.org/10.1016/j.tox.2010.07.010>.
- Akhtar, M.J., Ahamed, M., Alhadlaq, H.A., Khan, M.A.M., Alrokayan, S.A., 2015. Glutathione replenishing potential of CeO₂ nanoparticles in human breast and fibrosarcoma cells. *J. Colloid Interface Sci.* 453, 21–27. <https://doi.org/10.1016/j.jcis.2015.04.049>.

- Akhtar, M.J., Ahamed, M., Alhadlaq, H.A., Alshamsan, A., 2017. Nanotoxicity of cobalt induced by oxidant generation and glutathione depletion in MCF-7 cells. *Toxicol. Vitro* 40, 94–101. <https://doi.org/10.1016/j.tiv.2016.12.012>.
- Akhtar, M.J., Ahamed, M., Alhadlaq, H., 2020. Gadolinium oxide nanoparticles induce toxicity in human endothelial huvecs via lipid peroxidation, mitochondrial dysfunction and autophagy modulation. *Nanomaterials* 10, 1–18. <https://doi.org/10.3390/nano10091675>.
- Akhtar, M.J., Ahamed, M., Alhadlaq, H., 2022. CeO₂-Zn nanocomposite induced superoxide, autophagy and a non-apoptotic mode of cell death in Human Umbilical-Vein-Derived Endothelial (HUVE) Cells. *Toxics* 10, 250. <https://doi.org/10.3390/toxics10050250>.
- Akhtar, M.J., Ahamed, M., Alhadlaq, H., 2023. A selective toxicity of Pt-coated Au nanoparticles in cancerous MCF-7 cells over non-cancerous HUVE cells. *J. King Saud Univ. - Sci.* 35 (3), 102583.
- Atale, N., Gupta, S., Yadav, U.C.S., Rani, V., 2014. Cell-death assessment by fluorescent and nonfluorescent cytosolic and nuclear staining techniques. *J. Microsc.* 255, 7–19. <https://doi.org/10.1111/jmi.12133>.
- Battaglia, V., Compagnone, A., Bandino, A., Bragadin, M., Rossi, C.A., Zanetti, F., Colombatto, S., Grillo, M.A., Toninello, A., 2009. Cobalt induces oxidative stress in isolated liver mitochondria responsible for permeability transition and intrinsic apoptosis in hepatocyte primary cultures. *Int. J. Biochem. Cell Biol.* 41, 586–594. <https://doi.org/10.1016/j.biocel.2008.07.012>.
- Chattopadhyay, S., Dash, S.K., Tripathy, S., Das, B., Mandal, D., Pramanik, P., Roy, S., 2015. Toxicity of cobalt oxide nanoparticles to normal cells; An in vitro and in vivo study. *Chem. Biol. Interact.* 226, 58–71. <https://doi.org/10.1016/j.cbi.2014.11.016>.
- Crowley, L.C., Marfell, B.J., Scott, A.P., Waterhouse, N.J., 2016. Quantitation of apoptosis and necrosis by annexin V binding, propidium iodide uptake, and flow cytometry. *Cold Spring Harb. Protoc.* 2016, 953–957. <https://doi.org/10.1101/pdb.prot087288>.
- Fadok, V.A., Bratton, D.L., Frasch, S.C., Warner, M.L., Henson, P.M., 1998. The role of phosphatidylserine in recognition of apoptotic cells by phagocytes. *Cell Death Differ* 5 (7), 551–562.
- Fadok, V.A., Bratton, D.L., Rose, D.M., Pearson, A., Ezekewitz, R.A.B., Henson, P.M., 2000. A receptor for phosphatidylserine-specific clearance of apoptotic cells. *Nature* 405, 85–90. <https://doi.org/10.1038/35011084>.
- Fahmy, H.M., Ebrahim, N.M., Gaber, M.H., 2020. In-vitro evaluation of copper/copper oxide nanoparticles cytotoxicity and genotoxicity in normal and cancer lung cell lines. *J. Trace Elem. Med. Biol.* 60, 126481.
- Freese, C., Uboldi, C., Gibson, M.I., Unger, R.E., Weksler, B.B., Romero, I.A., Couraud, P. O., Kirkpatrick, C.J., 2012. Uptake and cytotoxicity of citrate-coated gold nanospheres: Comparative studies on human endothelial and epithelial cells. *Part. Fibre Toxicol.* 9, 23. <https://doi.org/10.1186/1743-8977-9-23>.

- Gieré, R., 2016. Magnetite in the human body: Biogenic vs. anthropogenic. *Proc. Natl. Acad. Sci. U.S.A.* 113 (43), 11986–11987.
- Jomova, K., Valko, M., 2011. Advances in metal-induced oxidative stress and human disease. *Toxicology* 283 (2-3), 65–87.
- Kobayashi, M., Shimizu, S., 1999. Cobalt proteins. *Eur. J. Biochem.* 261 (1), 1–9.
- Kong, I.C., Ko, K.S., Koh, D.C., Chon, C.M., 2020. Comparative effects of particle sizes of cobalt nanoparticles to nine biological activities. *Int. J. Mol. Sci.* 21, 1–19. <https://doi.org/10.3390/ijms21186767>.
- Lateef, R., Marhaba, Mandal, P., Ansari, K.M., Javed Akhtar, M., Ahamed, M., 2023. Cytotoxicity and apoptosis induction of copper oxide-reduced graphene oxide nanocomposites in normal rat kidney cells. *J. King Saud Univ. - Sci.* 35 (2), 102513.
- Li, J., Wang, J., Wang, Y.L., Luo, Z., Zheng, C., Yu, G., Wu, S., Zheng, F., Li, H., 2021. NOX2 activation contributes to cobalt nanoparticles-induced inflammatory responses and Tau phosphorylation in mice and microglia. *Ecotoxicol. Environ. Saf.* 225, 112725. <https://doi.org/10.1016/j.ecoenv.2021.112725>.
- Muñoz-Sánchez, J., Chánez-Cárdenas, M.E., 2019. The use of cobalt chloride as a chemical hypoxia model. *J. Appl. Toxicol.* 39 (4), 556–570.
- Ohkawa, H., Ohishi, N., Yagi, K., 1979. Assay for lipid peroxides in animal tissues by thiobarbituric acid reaction. *Anal. Biochem.* 95, 351–358. [https://doi.org/10.1016/0003-2697\(79\)90738-3](https://doi.org/10.1016/0003-2697(79)90738-3).
- Petronilli, V., Miotto, G., Canton, M., Colonna, R., Bernardi, P., Lisa, F.D., 1998. Imaging the mitochondrial permeability transition pore in intact cells. *Biofactors* 8 (3-4), 263–272.
- Rivet, C.J., Yuan, Y., Borca-Tasciuc, D.A., Gilbert, R.J., 2012. Altering iron oxide nanoparticle surface properties induce cortical neuron cytotoxicity. *Chem. Res. Toxicol.* 25, 153–161. <https://doi.org/10.1021/tx200369s>.
- Sabbioni, E., Fortaner, S., Farina, M., Del Torchio, R., Petrarca, C., Bernardini, G., Mariani-Costantini, R., Perconti, S., Di Giampaolo, L., Gornati, R., Di Gioacchino, M., 2014. Interaction with culture medium components, cellular uptake and intracellular distribution of cobalt nanoparticles, microparticles and ions in Balb/3T3 mouse fibroblasts. *Nanotoxicology* 8, 88–99. <https://doi.org/10.3109/17435390.2012.752051>.
- Sawai, H., Domae, N., 2011. Discrimination between primary necrosis and apoptosis by necrostatin-1 in Annexin V-positive/propidium iodide-negative cells. *Biochem. Biophys. Res. Commun.* 411, 569–573. <https://doi.org/10.1016/j.bbrc.2011.06.186>.
- Sukhanova, A., Bozrova, S., Sokolov, P., Berestovoy, M., Karaulov, A., Nabiev, I., 2018. Dependence of nanoparticle toxicity on their physical and chemical properties. *Nanoscale Res. Lett.* 13 (1) <https://doi.org/10.1186/s11671-018-2457-x>.
- Turrens, J.F., 2003. Mitochondrial formation of reactive oxygen species. *J. Physiol.* 552 (2), 335–344.
- Wan, R., Mo, Y., Feng, L., Chien, S., Tollerud, D.J., Zhang, Q., 2012. DNA damage caused by metal nanoparticles: involvement of oxidative stress and activation of ATM. *Chem. Res. Toxicol.* 25 (7), 1402–1411.
- Welder, A.A., 1992. A primary culture system of adult rat heart cells for the evaluation of cocaine toxicity. *Toxicology* 72 (2), 175–187.
- Yamada, K., 2013. Cobalt: its role in health and disease. *Met. Ions Life Sci.* 13, 295–320. https://doi.org/10.1007/978-94-007-7500-8_9.
- Yang, B., Chen, Y., Shi, J., 2019. Reactive oxygen species (ROS)-based nanomedicine. *Chem. Rev.* 119, 4881–4985. <https://doi.org/10.1021/acs.chemrev.8b00626>.
- Zheng, F., Luo, Z., Lin, X., Wang, W., Aschner, M., Cai, P., Wang, Y.L., Shao, W., Yu, G., Guo, Z., Wu, S., Li, H., 2021. Intercellular transfer of mitochondria via tunneling nanotubes protects against cobalt nanoparticle-induced neurotoxicity and mitochondrial damage. *Nanotoxicology* 15, 1358–1379. <https://doi.org/10.1080/17435390.2022.2026515>.